applied sciences

MDPI

Article

A New Macroscopic Traffic Flow Characterization Incorporating Traffic Emissions

Tanveer Qaiser [1], Ahmed B. Altamimi [2], Fayaz A. Khan [1], Mohammad Alsaffar [2], Abdulrahman Alreshidi [2], Khurram S. Khattak [3], Zawar H. Khan [4,*] and Wilayat Khan [5]

1 National Institute of Urban Infrastructure Planning, UET Peshawar, Peshawar 25000, Pakistan
2 College of Computer Science and Engineering, University of Ha'il, Ha'il 2440, Saudi Arabia
3 Department of Computer System Engineering, University of Engineering and Technology, Peshawar 25000, Pakistan
4 Department of Electrical and Computer Engineering, University of Victoria, Victoria, BC V8P 5C2, Canada
5 Department of Electrical and Computer Engineering, COMSATS University Islamabad—Wah Campus, Islamabad 45550, Pakistan
* Correspondence: khanz@uvic.ca

Abstract: Densely populated cities have led to increased traffic congestion and, consequently, increased greenhouse gas emissions from vehicles. Thus, it is important to develop traffic models to overcome congestion and increased air pollution. In the literature, traffic model characterizations rely predominantly on traffic dynamics and ignore traffic emissions. In this study, a new macroscopic model targeting traffic emissions and drivers' presumption based on traffic emissions is proposed to overcome traffic congestion and pollution. The traffic emissions characterization was based on the CO_2 data employed in the second traffic system. For the performance analysis, the results of the proposed and Zhang's traffic models were compared. The results were obtained using the ROE technique to predict traffic evolution. The scheme was implemented in MATLAB. Compared with Zhang's traffic model, the suggested traffic model based on emissions reflected traffic behavior more realistically.

Keywords: macroscopic flow; onboard diagnostic unit; CO_2; ROE technique

check for updates

Citation: Qaiser, T.; Altamimi, A.B.; Khan, F.A.; Alsaffar, M.; Alreshidi, A.; Khattak, K.S.; Khan, Z.H.; Khan, W. A New Macroscopic Traffic Flow Characterization Incorporating Traffic Emissions. *Appl. Sci.* **2023**, *13*, 5545. https://doi.org/10.3390/app13095545

Academic Editor: Carla Raffaelli

Received: 6 January 2023
Revised: 20 March 2023
Accepted: 18 April 2023
Published: 29 April 2023

Copyright: © 2023 by the authors. Licensee MDPI, Basel, Switzerland. This article is an open access article distributed under the terms and conditions of the Creative Commons Attribution (CC BY) license (https://creativecommons.org/licenses/by/4.0/).

1. Introduction

Air pollution refers to the presence in the air of substances that have a detrimental and poisonous impact on the environment and ecological system. The air pollutants include carbon monoxide, carbon dioxide, hydrocarbons, ammonia, sulfur dioxide, nitrous oxides, chlorofluorocarbons, and pollutant particulate matter. In urban areas, more solar energy is absorbed due to the type of land cover, which increases the environmental temperature.

In urban areas, extensive construction impedes air circulation and fresh air influx. Large buildings reduce wind speed, and the pollutant emissions from a large number of vehicles further intensify the increase in temperature. The ratio of pollution emission from the traffic can be lower than other urban sources, but it is large in the roadside vicinity. This problem is more severe in highly populated urban areas. Traffic pollution is not restricted to vehicles' exhausts. It also depends on the type of material used in the tires, engine age, type of fuel, fuel combustion, as well as the pavement material and its conditions. These factors impact human health.

Carbon monoxide, a colorless and odorless gas, is the most hazardous gas for human health; when inhaled, it combines with hemoglobin and reduces the capacity of blood to carry oxygen. Prolonged exposure to carbon monoxide causes slow death, as it reduces the oxygen levels in the body. It causes suffocation, nasal irritation, disorientation, dizziness, and headache. Sulfur dioxide has a strong smell and is produced by impurities present in the fuel. This causes irritation in the throat, eyes, and nose. High concentrations of this gas

can cause death. Sulfur dioxide contributes to the formation of sulfuric acid, which causes acidic rain, which, in turn, causes building corrosion and smog. The smog affects drivers' visibility and contributes to traffic accidents.

The growth of the global population has led to increased air pollution. In 2019, there were 4.2 million early deaths due to air pollution worldwide, with 223,000 deaths reported in Pakistan and 196,000 in the US [1]. Traffic emissions are a major contributor to air pollution. In 2020, traffic emissions were responsible for 45% of the pollution in the US [2], while in 2017, the greenhouse emissions in Europe were at 72%. Passenger vehicles produced 44% of greenhouse gases in Europe, while heavy transport caused 9% [3]. In China, road vehicles are responsible for about 80% of CO emissions and 40% of NO_x emissions [4]. Urban traffic emissions have increased air pollution and reduced the quality of air, which harms not only the human body but also the ecological system.

Particulate matter can have a solid or liquid form and includes engine wear, heavy metals, hydrocarbons, and sulfur and nitrogen composites. Particulate matter production is higher in diesel engines than in gasoline engines. The vehicles listed as zero pollution emission mostly use electricity charging, and electricity production has its own impact on the environment.

CO_2 emitted from fossil fuels contributes about 65% to global greenhouse gas emissions (GHGs). In 2020, CO_2 emitted from direct human involvement impacted forestry, contributing 11% of GHGs. Globally, 16% of CH_4, 6% of N_2O, and 2% of fluorinated gases (F-gases) contribute to GHGs [2]. Harmful traffic emissions not only reduce the air quality but also affect natural biological systems. It is therefore vital to characterize traffic emissions to improve air quality and reduce emission-associated risks. Different traffic emission characterizations are being established to assess traffic pollutants.

Traffic emissions can be assessed using vehicle emission exhaust. The usual method to obtain vehicle emissions is calculating the pollutants ratio based on vehicle mobility [5]. Pollution emission from a single vehicle is used as the pollutant ratio. It gives the pollutant quantity after 1 km of travel and considers the engine load, vehicle acceleration, and speed. The number of kilometers driven, trips made from origin to destination, and the duration of travel are considered as vehicle activity [6]. The result for the total emissions using the emission factor and vehicle's activity is presented as

$$\text{Total traffic emissions} = \text{Vehicle Activity} \times \text{pollutant ratio}$$

In the literature, different methods are employed to assess traffic emission inventories and fuel consumption, characterizing the traffic situation, average speed, cycle variable, emissions, and instantaneous emission models [7]. Speed characterization considers the different road speeds. In 1998, Ahn used a mathematical regression model and the vehicle speed and acceleration to assess the emission ratio and fuel consumption [5]. In 1978, Evans and Herman [8] used the average speed model to estimate the fuel consumption ratio from trips traveled over a road segment. This approach could not estimate fuel consumption on small road segments and for traffic at speeds faster than 60 km/h [9]. They could be obtained by estimating fuel consumption and traffic pollutants instantaneously.

The level of traffic emissions from the vehicle's engine at the start depends on the engine temperature, which is low in engines that are inactive for extended periods. Cold engines produce high emissions during starting, while the warmer engines have lower emissions at startup. Evaporative emissions are due to fuel evaporation when the vehicle's engine is hot at the end of a trip. Models for inventorying and estimating traffic emissions, such as ARTEMIS [10], calculate evaporative emissions, as well as different emissions from hot- and cold-start engines. The ARTEMIS model requires detailed information on the vehicle composition and the distance traveled (vehicle activity) to provide more consistent data on the vehicle and diverse driver behaviors. However, the model requires substantial data validation and collection resources, which have a large financial impact.

As the number of vehicles increases due to population growth and complex urban traffic circumstances, traffic pollutant modeling becomes more important in reducing air pollution (congestion). Some organizations struggle to meet the national air quality and transportation emissions goals. More realistic traffic flow models are needed to characterize traffic emissions more correctly. As a result, data on traffic emissions and flow characteristics are maintained consistently. In this paper, a more realistic second-order traffic model based on traffic emissions is proposed.

Traffic emissions are characterized at different levels. Microscopically, the instantaneous engine revolution per minute, acceleration, and speed of individual vehicles are considered. Macroscopically, the aggregate flow, density, and speed are considered. In order to forecast traffic emissions and flow, the authors of this paper used the microscopic traffic emission parameters in a macroscopic traffic model that was easy to implement. The vehicles' speed, mass airflow, the ratio of fuel to air, and the engine speed were obtained through onboard diagnostic units.

The traffic models are classified as macroscopic, microscopic, and mesoscopic. The macroscopic models consider the speed, the number of vehicles on a road segment (traffic density), and traffic flow. This model type provides the average changes in traffic parameters over the length of the road. The temporal and spatial traffic evolutions are also characterized. These types of models are developed using partial differential equations systems. This paper considered aggregate flow (macroscopic) models in conjunction with instantaneous emission models to characterize the average pollutants' emissions.

The second-order macroscopic systems of aggregate traffic behavior are based on traffic conservation: acceleration and deceleration. The first macroscopic traffic model of this type was developed by Richards, Lighthill, and Whitham [11]. The second element was based on the presumption of changes by a driver (anticipation) and speed alignment at those changes (relaxation) to attain equilibrium conditions. Payne and Whitham (PW model) were the first to propose a second-order traffic system with anticipation and relaxation terms. That model estimated that at traffic changes, vehicles had uniform interactions. Consequently, traffic density and speed progressed idealistically. Realistically, the model should have considered the presumptions of drivers. In 1996, Helbing improved the gas kinetic theory (GKT) model with the help of numerical schemes. That characterization employed velocity and density correlations and helped estimate complicated traffic changes. Their model provided an anisotropic traffic progress [12]. In 2010, Caligaris et al. suggested numerical stability conditions to estimate traffic progress accurately with the PW model. In 2015, Bosire et al. implemented Zhang's characterization in Kenya to correctly estimate traffic progress on a 500 m road segment, which justified the use of aggregate traffic parameters [13]. In 2017, Mohan and Ramadurai improved the PW model by incorporating the area occupancy parameter into the model instead of traffic density. The model captured the bottleneck effect more accurately than previous models but ignored the drivers' anticipation of the traffic conditions [14]. In 2016, Khan and Gulliver improved the PW model by considering the traffic speed changes, which improved the model's inaccurate traffic estimation [15]. They also suggested another new macroscopic model that considered traffic speed management and the drivers' physiological and psychological states and reactions. According to their assumptions, the drivers' anticipation should be characterized based on physiology and psychology. Khan and Gulliver improved the model by incorporating the traffic transition velocities acquired during traffic alignment [16]. Zhang [17], Aw Rascle [18], Daganzo [19], and Berg et al. considered mathematical techniques to reduce the large changes flow, which was unrealistic. Khan and Gulliver's models improved the traffic characterization based on the traffic's physical parameters, resulting in more realistic and accurate representations of the traffic changes.

2. Methodology

The methodology of this study consisted of choosing a road, including the start and destination locations for a round trip, the vehicle's instantaneous fuel consumptions and emissions acquisition, the maximum traffic density estimation, and a CO_2 instantaneous regression model. The CO_2 regression model was incorporated into the second-order traffic system to characterize traffic behavior. The proposed model was then compared with Zhang's model for performance analysis. The models were discretized with the ROE decomposition scheme [16] in MATLAB. The proposed methodology is shown in Figure 1.

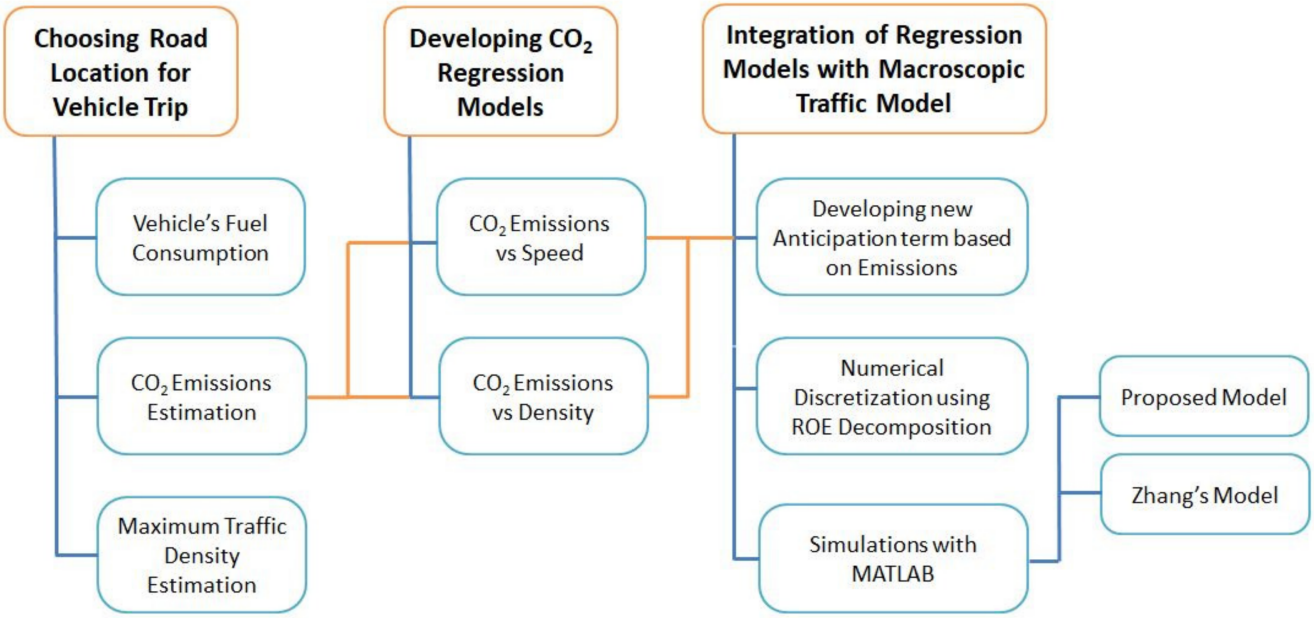


Figure 1. The research methodology. The colored lines show the microscopic and macroscopic view of the idea implemented.

2.1. Instantaneous Emissions Acquisition

Pollution emissions from vehicle exhausts during a trip were obtained using a dynamometer. This is the usual method to characterize instant emissions through the engine load, acceleration, and speed of vehicles. These data were utilized to obtain emissions regression models.

In this study, a smartphone Android app, "BotlnckDectr" [20], was employed to measure the CO_2 pollutant emitted when a vehicle traversed a route. The route selected for this study started at 33.9761° N, 71.4453 E° and ended at 34.0020° N, 71.4851 E°. The origin of the route was Phase 2, Hayatabad, and the destination was the University of Engineering and Technology (UET) Peshawar, KPK, Pakistan; the morning trip was from 08:39 a.m. to 08:54 a.m., as shown in Figure 2. In the evening, the trip route was from UET Peshawar to Phase 2 Hayatabad, Peshawar, from 05:20 p.m. to 05:35 p.m., as shown in Figure 3. The evening trip was observed on Monday, 19 January 2020. The total length of the morning route was 7.7 km, and the evening route was 7.1 km long. In the morning, the total travel time on this route was 14 min, while the evening trip lasted 17 min. The congested traffic occurred on the N5 road, indicated with a red color in Figure 3. The blue color indicates the free flow and smooth traffic. The traffic flow was heterogeneous, with no lane discipline followed by the drivers. Data and images in Figures 2 and 3 are courtesy of Google Maps. The route was tested during weekdays from 19 January 2021 to 22 January 2021.

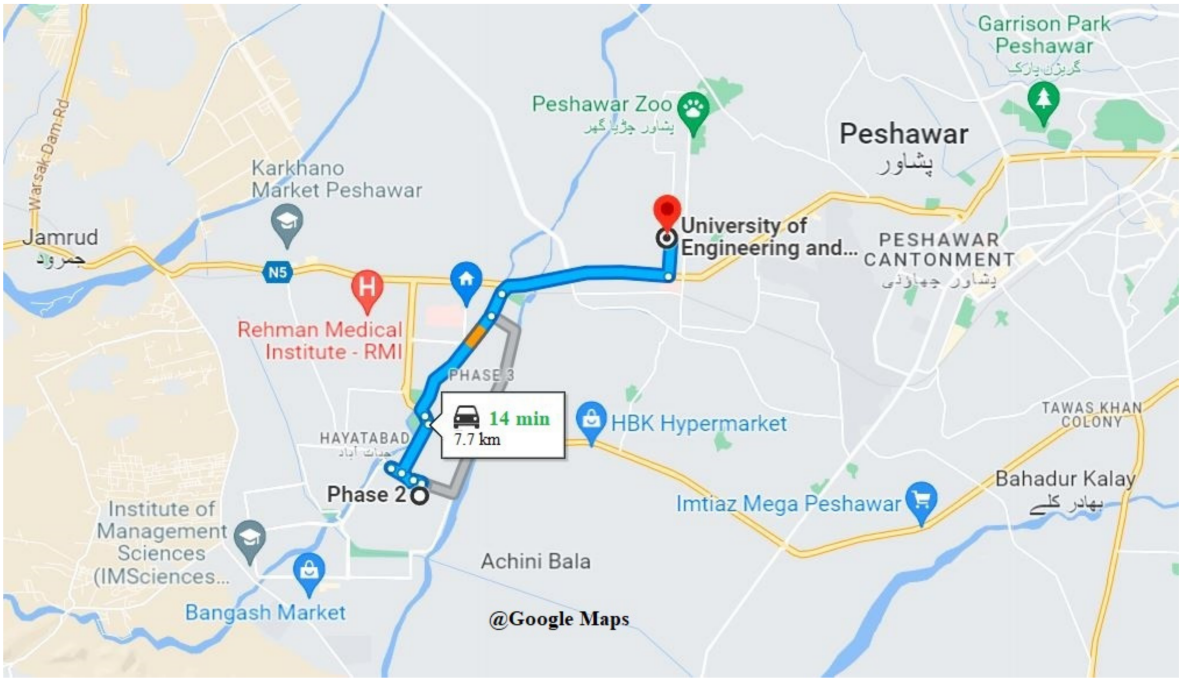


Figure 2. The morning trip (33.9761° N, 71.4453 E° to 34.0020° N, 71.4851 E°) from Phase 2, Hayatabad, Peshawar to University of Engineering and Technology, Peshawar, KPK, Pakistan.

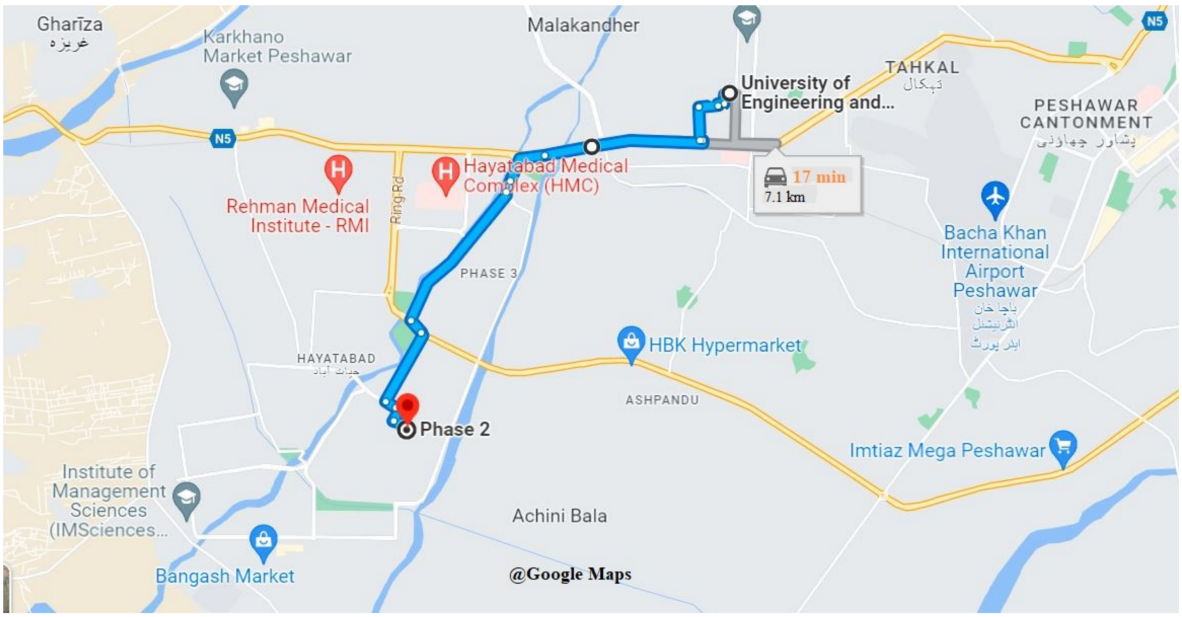


Figure 3. The evening trip (34.0020° N, 71.4851 E° to 33.9761° N, 71.4453 E°) from the University of Engineering and Technology, Peshawar to Phase 2, Hayatabad, Peshawar, KPK, Pakistan.

2.2. Data Collection with Onboard Instrumentation

BotlnckDectr's system block diagram is shown in Figure 4 [20]. The onboard diagnostic (OBD) unit is a transportable device in vehicles manufactured after 1996 [20]. In this experiment, OBD-II collected the data from the engine control unit (ECU) of a 1600 cc Toyota Corolla manufactured in 2015 [20,21]. The obtained data included engine speed in revolution per minute, speed, mass airflow (MAF) intake, temperature, and air-to-fuel ratio (AFR). Mass airflow ($\frac{g}{s}$) is the rate of air entering in a vehicle's engine. The AFR was $\frac{14.7\ g}{1\ g}$ for gasoline. Engine sparks at the intake air temperature and fuel were injected for

the best performance. Usually, the intake air temperature was 30 to 70 °C. An ELM 327 adapter (OBD-II) was utilized in this research to transmit the data from the vehicle's ECU. OBD-II transferred data at 5 s through Bluetooth connectivity from the ECU to BotlnckDectr (Android application). In real time, BotlnckDectr received sensor data from the vehicle. In addition to the acquired data, the time and location of a vehicle from a smartphone's GPS were communicated through a cellular network to Amazon Web Services DynamoDB. Amazon Web Service (AWS) is a subsidiary of Amazon that provides a suite of cloud computing services, including storage, computing power, and databases. These services are offered over the internet, allowing organizations to build and run applications and store data in the cloud rather than on physical servers located in their own facilities [20].

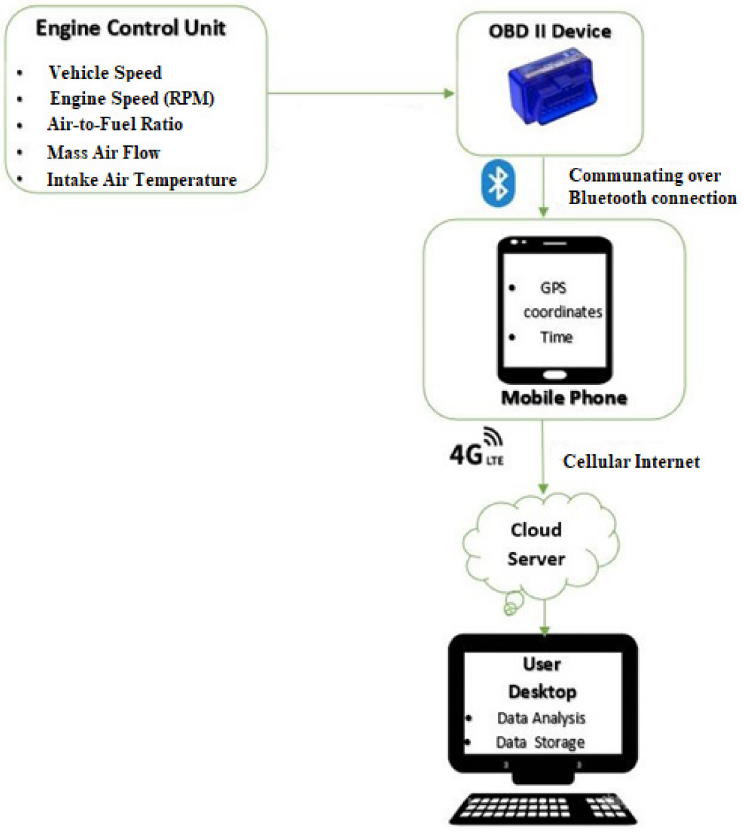


Figure 4. Vehicle's data acquisition methodology [20].

Our choice of AWS was influenced by multiple design considerations, including AWS' reliability and scalability. However, other important considerations were communication and data security. AWS provides a wide range of services for data protection both while in transit (as it travels to AWS) and at rest (while stored at AWS) through different services such as identity and access management (IAM), certificate manager, Amazon GuardDuty, to name a few [22]. All data from remote devices were transmitted to AWS through a TLS connection using HTTPS, MQTT, and WebSocket protocols, ensuring security by default while in transit.

2.3. CO_2 Emissions

CO_2 is one of the significant vehicle emissions and is continuously emitted from the reaction of oxygen with the burning of the carbon content in the fuel. The atomic mass of CO_2 from oxygen and carbon [23] is

$$[CO_2]_\mu = 12_\mu + (2 \times 16_\mu) = 44_\mu, \quad (1)$$

where 16 and 12 are the atomic masses of oxygen and carbon, respectively, and μ denotes atomic masses. In a combustion process, CO_2 produced from 1 kg of C in the fuel is [23]

$$\frac{(12+16+16)}{12} \approx 3.67 \text{ kg } CO_2, \tag{2}$$

The carbon content in gasoline is 87% [23]. Thus, the total CO_2 emission from burning gasoline is

$$E_{CO2} = 3.67 \times 0.87 \times \text{gasoline weight}, \tag{3}$$

where E denotes the emission. From Equation (3), the mass of carbon dioxide in 1 kg of gasoline is

$$E_{CO2} = 3.19 \text{ [kg/(1 kg fuel)]}. \tag{4}$$

The density of gasoline fuel is 0.73 $\left[\frac{\text{kg}}{\text{L}}\right]$ [23]; therefore, the CO_2 emissions from 1 L of gasoline fuel combustion are

$$E_{CO2} = 3.19 \times 0.73 = 2.3 \text{ [kg/(1 L fuel)]}. \tag{5}$$

From the consumption of 1 L of gasoline, 2.3 kg of carbon dioxide is formed. To obtain CO_2 emissions in a kilometer, Equation (5) is divided by the KPL:

$$E_{CO2} = [(2.3 \text{ [kg/l]})/(\text{KPL [km/L]})]. \tag{6}$$

The KPL is the number of kilometers per liter of fuel and is given as

$$\text{KPL} = (\text{Speed of Vehicle})/\text{LPH}, \tag{7}$$

where LPH is the liters of fuel per hour and is given as

$$\text{LPH} = \text{GPH} \times 3.75, \tag{8}$$

where GPH is the gallons of fuel per hour and is given as

$$\text{GPH} = \text{MAF} \times 0.805. \tag{9}$$

From Equations (7)–(9) and (6), for CO_2 emissions per km are obtained as

$$E_{CO2} = (2.3 \times \text{MAF} \times 0.805 \times 3.75)/(\text{Speed of Vehicle}) \tag{10}$$

In this paper, vehicle speed and MAF were calculated from the vehicle's ECU obtained with the OBD-II device. Table 1 shows the units and the symbols used to estimate carbon dioxide gas emissions.

Table 1. Summary of all the units used in CO_2 emissions estimation.

Symbol	Units	Description
$[CO_2]_\mu$	Amu	Atomic mass of carbon dioxide
E_{CO2}	kg CO_2/km	Carbon dioxide gas emissions
KPL	km/L	Number of kilometers traveled per liter of fuel
LPH	L/h	Liters of fuel consumed per hour
GPG	ga/h	Gallons of fuel consumed per hour
MAF	g/s	The rate of air entering in the vehicle's engine
V	km/h	The speed of the vehicle
ρ	veh/length	The density of traffic
RPM	r/min	The revolutions of the engine per minute

2.4. Maximum Traffic Density

The maximum density ρ_n at time n was obtained from the data acquired at 5 s intervals from the vehicle speed $V_n(\rho)$. Greenshield's velocity distribution [24] was utilized to obtain

$$\rho_n = \left(1 - \frac{V_n(\rho)}{v_m}\right)\rho_m. \tag{11}$$

where v_m and ρ_m are, respectively, maximum speed and density.

The location to determine the maximum speed and density was University Road, Peshawar, KPK, Pakistan. This is a traffic bottleneck and is considered to have the worst traffic flow. Figure 5 shows the location where the maximum density was obtained, a 32 m long road segment with 3 lanes. The vehicles were not following lane control. Along the 32 m segment, cameras were fixed at egress and ingress. The traversing time of individual vehicles was recorded at egress and ingress to attain the desired speed, given as

$$v = \frac{\text{length}}{\text{egress time} - \text{ingress time}}. \tag{11a}$$



Figure 5. Maximum traffic density was calculated at University Road Peshawar, KPK, Pakistan, 34.0020° N, 71.4851 E°.

Then, the total number of vehicles for that duration was counted to obtain the maximum traffic density, given as

$$\rho = \frac{\text{number of vehicles}}{\text{section length}} \tag{11b}$$

The traffic density was assessed for 1800 s. A total of 340 observations (data points) were made, and the observed ρ_m was 500 veh/km to estimate ρ_n at n from (11).

2.5. Data Analysis

The data collected from the vehicle through the OBD-II device contained 130 data points (observations) for each day. Table 2 provides the quantitative statistics on the data points from the recorded parameters. Observations were obtained at 5 s intervals during the morning and evening trips for a period of 4 days. The engine's revolution per minute, vehicle equilibrium speed, AFR, and MAF were acquired for both trips. Figure 6 shows the vehicle speeds recorded during the morning trips. The maximum morning speed was

72 km/h, and the minimum was 1 km/h. Figure 7 illustrates the evening trip's temporal changes in vehicle speeds with the minimum equilibrium observed speed of 2 km/h and the maximum of 69 km/h. The minimum equilibrium speed observed during morning and evening trips during the 4 days was 1.00 km/h, while the maximum was 72 km/h. Figure 8 demonstrates the temporal changes in MAF in a trip originating from Phase 2, Hayatabad, observed over 4 days. The MAF in the morning trip varied from 0.01 g/s to 25.65 g/s. Figure 9 demonstrates the temporal changes in MAF in a trip originating from UET Peshawar, observed over 4 days. The minimum mass airflow rate observed in the evening trip was 0.15 g/s, while the maximum was 43.52 g/s. The engine's rpm varied from 643 to 2113 rev/min. The intake air temperature varied from 16 to 36 °C. The air/fuel ratio of gasoline fuel was 1.

Table 2. Characteristic of all the parameters during morning and evening.

Days	Parameter	Min	Max	Mean	Standard Deviation	Variance
Day 1	Engine RPM	643.00	2113.00	1372.20	423.25	179,143.69
	Intake air temp	16.00	36.00	24.50	4.95	24.47
	AFR	1.00	1.00	1.00	1.00	1.00
	MAF	2.00	22.82	5.49	4.49	20.14
	Equilibrium speed (velocity)	2.00	62.00	21.48	17.10	292.44
Day 2	Engine RPM	641.00	2499.00	1391.30	455.38	207,373.68
	Intake air temp	18.00	33.00	24.16	3.84	14.78
	AFR	1.00	1.00	1.00	1.00	1.00
	MAF	0.11	25.65	5.91	6.01	36.15
	Equilibrium speed (velocity)	2.00	72.00	24.14	17.93	321.49
Day 3	Engine RPM	640.00	2434.00	1402.80	473.68	224,369.17
	Intake air temp	25.00	35.00	29.98	2.55	6.51
	AFR	1.00	1.00	1.00	1.00	1.00
	MAF	1.00	23.00	6.17	5.27	27.78
	Equilibrium speed (velocity)	1.00	63.00	23.54	16.49	271.82
Day 4	Engine RPM	640.00	2626.00	1346.46	448.86	201,472.88
	Intake air temp	21.00	32.00	24.51	2.43	5.89
	AFR	1.00	1.00	1.00	1.00	1.00
	MAF	0.01	43.52	7.32	8.66	74.98
	Equilibrium speed (velocity)	2.00	69.00	25.70	18.04	325.62

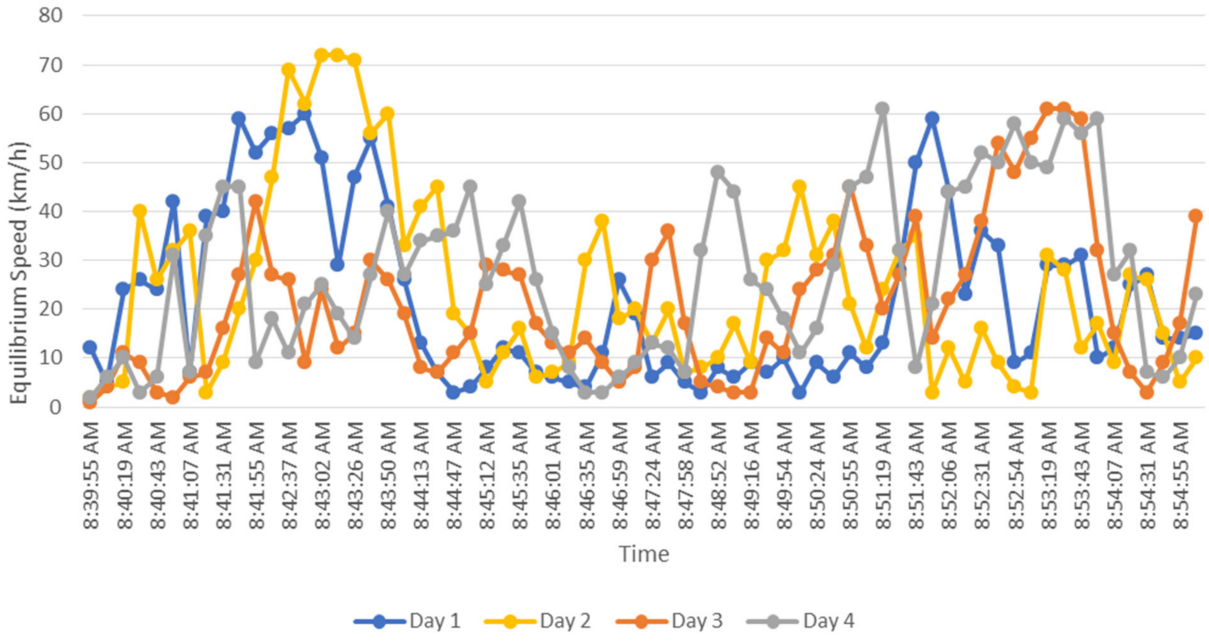


Figure 6. Variations of equilibrium speed (velocity) in the morning.

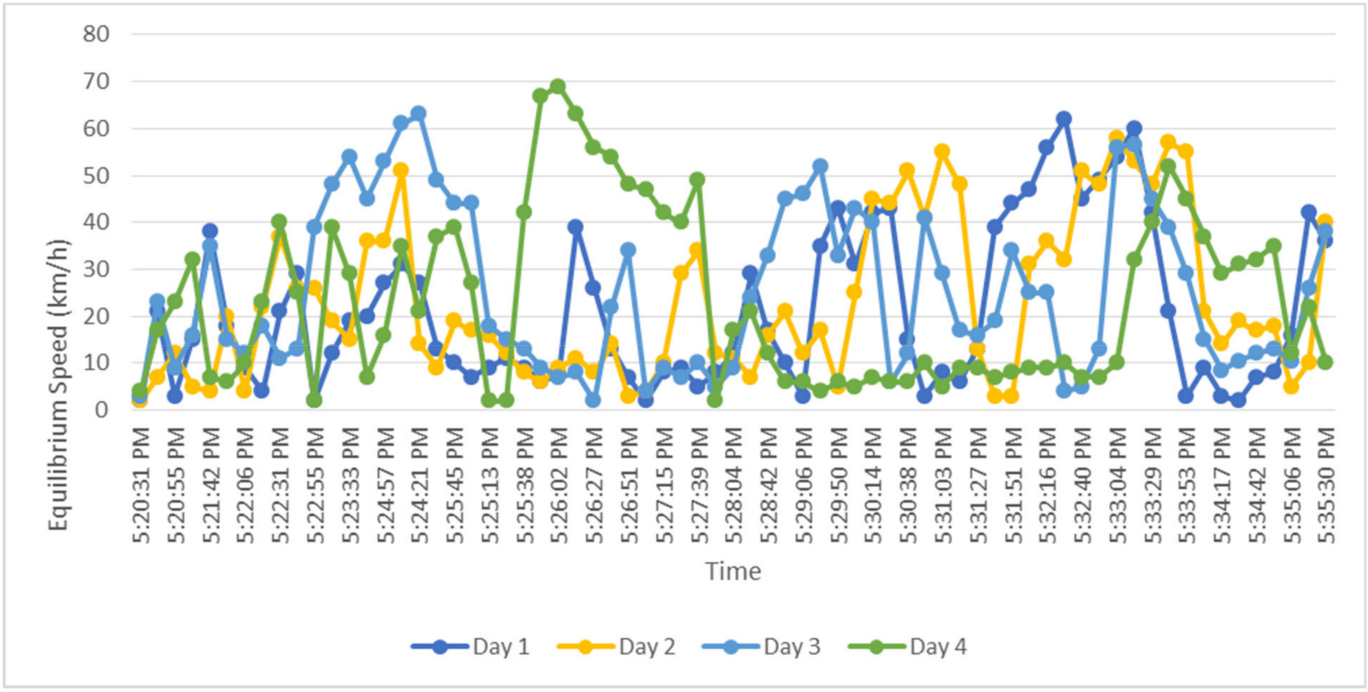


Figure 7. Variations of equilibrium speed (velocity) in the evening.

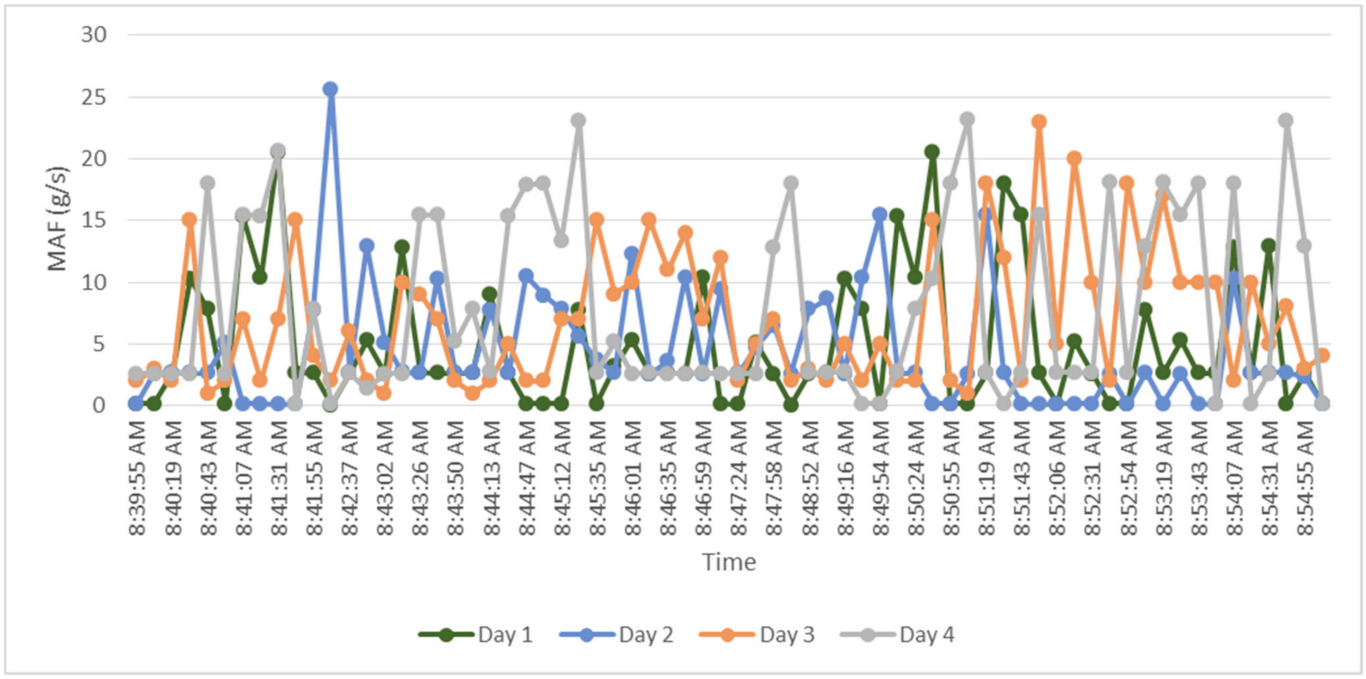


Figure 8. Variations of MAF in the morning.

The quantitative statistics of all parameters collected from the test vehicle using OBD II during the morning and evening are summarized in Table 2.

Table 3 shows the quantitative statistics of CO_2 emissions, speed, and density f from day 1 to day 4 of data collection. The CO_2 emissions were calculated using Equation (10), the density was calculated using Equation (11), and the speed was obtained from Table 2.

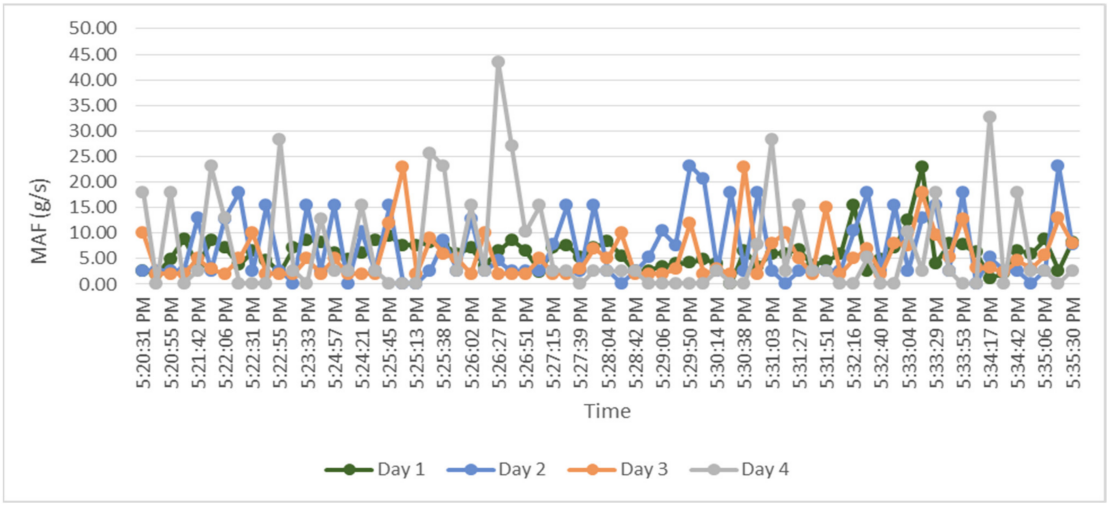


Figure 9. Variations of MAF in the evening.

Table 3. Characteristic of all regression model parameters during morning and evening trips.

Days	Parameter	Min	Max	Mean	Standard Deviation	Variance
Day 1	CO_2 emissions (kg CO_2/km)	0.02	17.84	3.98	3.24	10.51
	Speed (km/h)	2.00	62.00	21.48	17.10	292.44
	Density (veh/km)	0	483.87	331.35	135.47	18,353.16
Day 2	CO_2 emissions (kg CO_2/km)	0.02	32.15	2.94	5.60	31.33
	Speed (km/h)	2.00	72.00	24.14	17.93	321.49
	Density (veh/km)	32.26	483.87	314.52	135.77	18434
Day 3	CO_2 emissions (kg CO_2/km)	0.21	13.89	3.74	3.58	12.84
	Speed (km/h)	1.00	63.00	23.54	16.49	271.82
	Density (veh/km)	8.06	491.94	325.97	126.85	16,091.55
Day 4	CO_2 emissions (kg CO_2/km)	0.22	13.31	2.66	3.11	9.65
	Speed (km/h)	2.00	69.00	25.70	18.04	325.62
	Density (veh/km)	0	484.13	282.95	145.27	21,102.56

3. Regression Models for Emissions

The regression method was employed to estimate CO_2 emissions using the density and vehicle speed, as shown in Table 3. The various regression models for CO_2 emissions are shown in Table 4 against the equilibrium velocity (speed) and density data and their R^2 values. R^2 is a measure of goodness of fit to a model. The higher the value of R^2, the closer the model is to the data.

Table 4. Regression summary of various emission models against speed and density.

Emissions vs. Speed			Emissions vs. Density		
Type of Model	**Regression Model**	**R^2**	**Type of Model**	**Regression Model**	**R^2**
Linear	$E_{CO2} = 7.032 - 0.1461v(\rho)$	57%	Linear	$E_{CO2} = -2.026 + 0.02236\rho$	57%
Quadratic	$E_{CO2} = 13.15 - 0.5979v(\rho) + 0.006718v(\rho)^2$	75%	Quadratic	$E_{CO2} = 1.899 - 0.03599\rho + 0.000157\rho^2$	75%
Cubic	$E_{CO2} = 10.25 - 0.6289v(\rho) + 0.0133v(\rho)^2 - 0.00008v(\rho)^3$	76%	Cubic	$E_{CO2} = 1.475 - 0.00095\rho - 0.000073\rho^2 + 0.00000001\rho^3$	76%

Table 4 shows the quantitative statistics for various variables of regression models collected during the four days' morning and evening trips. These variables include the CO_2

emissions (kg CO_2/km), speed of the vehicle (km/h), and the density of traffic (veh/km). The variance in CO_2 emission data was largest on day 2 and lowest on day 4. The variance in speed data was largest on day 4 and smallest on day 3. The variance in density data was the largest on day 4 and smallest on day 3. Overall, the data collected on day 3 for the variables of the regression models showed less variance. The maximum emissions were recorded during day 2 of data collection.

3.1. Regression Model 1

The vehicle speed was used as a predictor to regress CO_2 emissions as follows:

$$E_{CO_2} = 13.15 - 0.5979\,\nu(\rho) + 0.006718\,\nu(\rho)^2, \tag{12}$$

which can estimate CO_2 emissions from the equilibrium speed. In other words, CO_2 emissions were based on the speed and could be controlled by optimizing traffic speed. Figure 10 shows the trend line of Equation (12).

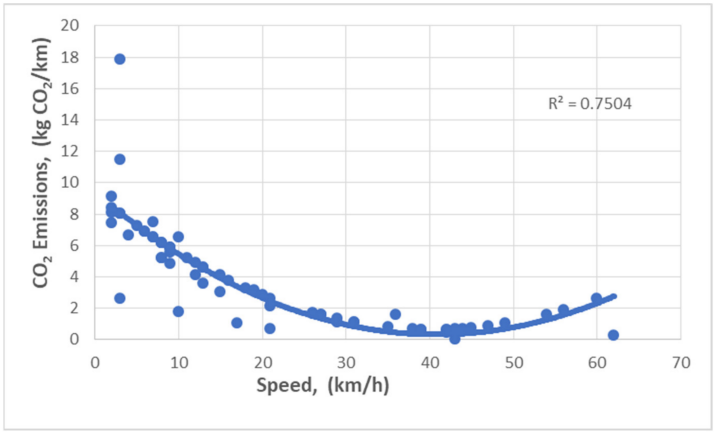


Figure 10. CO_2 emissions' trend line of Equation (12) with changes in speed.

3.2. Regression Model 2

Traffic density was used as a predictor to regress CO_2 emissions as follows:

$$E_{CO_2} = 1.899 - 0.03599\rho + 0.000157\rho^2, \tag{13}$$

which can estimate CO_2 emissions from the traffic density. In other words, CO_2 emissions from the density could be characterized to determine traffic emissions. Figure 11 shows the trend line of Equation (13).

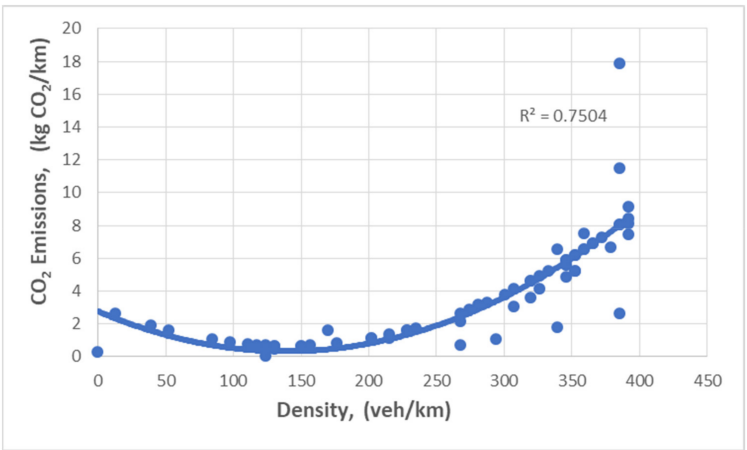


Figure 11. CO_2 emissions' trend line of Equation (13) with changes in density.

4. Suggested Traffic Model Based on Traffic Emissions

Zhang's traffic characterization is

$$\frac{\partial \rho}{\partial t} + \frac{\partial (\rho v)}{\partial x} = 0 \tag{14}$$

$$\frac{\partial v}{\partial t} + \frac{v \partial v}{\partial x} + \rho \left(\frac{dv(\rho)}{d\rho} \right) \frac{\partial \rho}{\partial x} = \frac{v(\rho) - v}{\tau}, \tag{15}$$

which assumes that the flow is smooth with no exits and entrances to a road when deceleration and acceleration do not occur. In the case of transitions, Equation (15) can calculate traffic changes. A driver's presumption considers the density changes. That is, speed changes corresponds to changes in density. The speed changes occur during relaxation time τ and adapt to equilibrium speed $v(\rho)$. This model ignores the impact of emissions on speed and traffic density. However, traffic emission modeling and mitigation are equally important to improve the environmental quality of the road surroundings. Equilibrium speeds are characterized to confirm a traffic situation [25]. For ease of implementation, Greenshield's equilibrium speed Equation (11) was employed in the proposed model.

For effective traffic emissions management, traffic characterization must consider emission fluctuations. The pollutant emissions correspondingly vary with speed adjustments, and more fluctuation is experienced at transitions. To model the traffic more realistically, CO_2 emissions were regressed from the acquired density and speed. From Equations (12) and (13), CO_2 emissions fluctuated as the speed and density varied. Speed changes in traffic are density-dependent. A large fluctuation in speed occurs as a large variation in density occurs. Similarly, changes in velocity are small for small variations in density. A driver presumes speed changes while observing the changes in density. Consequently, considering the changes in emission with speed and density from (12) and (13), respectively, can result in a driver's presumption to effectively manage emissions. That is, considering the equilibrium speed $v(\rho)$, (12) results in

$$\frac{dE_{CO_2}}{dv(\rho)} = -0.5979 + 0.0134\, v(\rho). \tag{16}$$

Changes in equilibrium velocity distribution with emissions from $\frac{dE_{CO_2}}{dv(\rho)}$ result in

$$\frac{dv(\rho)}{dE_{CO_2}} = \frac{1}{-0.5979 + 0.0134\, v(\rho)}. \tag{17}$$

Changes in vehicle emission with density from Equation (13) result in

$$\frac{dE_{CO_2}}{d\rho} = -0.03599 + 0.000314\, \rho. \tag{18}$$

The speed changes with density having an impact on vehicle emissions are obtained with Equations (16) and (18) as

$$\frac{dv(\rho)}{d\rho} = \frac{-0.03599 + 0.000314\rho}{-0.5979 + 0.0134\, v(\rho)}. \tag{19}$$

This means that equilibrium speed changes are small at a faster speed and large at a lower speed. In other words, the tendency toward changes in equilibrium speed is more prominent in congested traffic than in free flow. Furthermore, the changes in equilibrium speed in a higher traffic density are large, and they are small in a lower density. Equation (19) suggests that emission variations are more significant in congested, high-density traffic, as emissions are larger in slower traffic. To include the emissions' impact in Zhang's model, $\frac{dv(\rho)}{d\rho}$ from Equation (19) is substituted with (15).

The distance h between vehicles is small in congested traffic and larger in free flow. In other words, as the distance between the vehicles reduces, density increases, resulting in higher emissions. That is,

$$\rho = \frac{1}{h}. \tag{20}$$

Drivers try to keep a safe distance h_s in addition to the distance required to maneuver a vehicle to prevent accidents. The distance required to maneuver a vehicle depends on speed v and relaxation time τ At higher speeds, the control distance covered is larger than at the slower speed.

Further, h takes the form

$$h = h_s + \tau v. \tag{21}$$

From Equation (21), Equation (20) becomes

$$\rho = \frac{1}{(h_s + \tau\, \nu)}. \tag{22}$$

Then, from Equations (19) and (22), the coefficient $\rho\frac{dv(\rho)}{d\rho}$ of $\frac{\partial\rho}{\partial x}$ (driver anticipation) in Equation (15) becomes

$$\rho\frac{dv(\rho)}{d\rho} = \left(\frac{-0.03599 + 0.000314\rho}{-0.5979 + 0.0134v(\rho)}\right)\left(\frac{1}{h_s + \tau v}\right). \tag{23}$$

Combining Equation (23) with (15), the proposed model based on CO_2 emissions results in

$$\frac{\partial\rho}{\partial t} + \frac{\partial(\rho v)}{\partial x} = 0 \tag{24}$$

$$\frac{\partial v}{\partial t} + \frac{v\partial v}{\partial x} + \left(\frac{-0.03599 + 0.000314\rho}{-0.5979 + 0.0134v(\rho)}\right)\left(\frac{1}{h_s + \tau v}\right)\frac{\partial\rho}{\partial x} = \frac{-v}{\tau}. \tag{25}$$

Equations (24) and (25) are the proposed traffic characterizations that consider traffic emissions. Equation (24) is the same as Equation (14) [25]. The speed and density estimated with the suggested model can forecast CO_2 emissions using the regression models developed in Section 3.

5. ROE Discretization of Models

A numerical decomposition of traffic models is required to divide the continuous functions into small discrete parts to obtain algorithms for the numerical simulations. Many schemes are used to decompose traffic models, including finite-volume methods, finite-difference methods, and higher-resolution schemes. The ROE discretization scheme [26–28] was used to implement the proposed and Zhang's models in MATLAB to provide more accurate results for traffic behavior. This high-resolution scheme solved the partial differential systems with large changes more accurately. For a more accurate traffic behavior with large changes, an entropy fix was employed [16].

The conserved traffic model in vector form is

$$\mathrm{U}_t + \mathrm{f(u)}_x = \mathrm{R}. \tag{26}$$

where U represents data variables, f(u) represents the function vector, and R represents the source vector. Subscripts x and t show the spatial and temporal gradients of the data variables, respectively.

For the conserved form of the suggested model, Equation (24) is multiplied by v, which gives

$$v\frac{\partial(\rho)}{\partial t} + v\frac{\partial(\rho v)}{\partial x} = 0, \tag{27}$$

and multiplying Equation (25) by ρ gives

$$\frac{\rho\partial v}{\partial t} + \frac{\rho v\partial v}{\partial x} = -\frac{(-0.03599 + 0.000314\rho)}{(-0.5979 + 0.0134v(\rho))}\frac{1}{(h_s + \tau v)}\frac{\partial(\rho)}{\partial x} + \frac{\left(v_m\left(1 - \frac{\rho}{\rho_m}\right) - v\right)}{\tau} \tag{28}$$

Combining Equations (27) and (28) gives

$$\begin{array}{c} \frac{\rho\partial v}{\partial t} + \frac{\rho v\partial v}{\partial x} + v\frac{\partial(\rho)}{\partial t} + v\frac{\partial(\rho v)}{\partial x} \\ = -\frac{(-0.03599+0.000314\rho)}{(-0.5979+0.0134v(\rho))}\frac{1}{(h_s+\tau v)}\frac{\partial(\rho)}{\partial x} + \frac{\left(v_m\left(1-\frac{\rho}{\rho_m}\right)-v\right)}{\tau} \end{array} \tag{29}$$

Rearranging Equation (29) gives

$$(\rho v)_t + \left[\frac{\left(\rho v\right)^2}{\rho} + \left(\frac{-0.03599 + 0.000314\rho}{-0.5979 + 0.0134v(\rho)}\right)\frac{1}{(h_s + \tau v)}\rho\right]_x = \frac{\rho\left(v_m\left(1 - \frac{\rho}{\rho_m}\right)\right) - v}{\tau}. \tag{30}$$

The subscripts t and x denote the temporal and spatial gradients, respectively. This is the conserved form of the proposed model from Equation (25). The proposed model from Equations (24) and (30) in the vector form of Equation (26) is

$$\begin{bmatrix}\rho \\ \rho v\end{bmatrix} + \begin{bmatrix}\rho v \\ \frac{(\rho v)^2}{\rho} + \left(\frac{-0.03599+0.000314\rho}{-0.5979+0.0134v(\rho)}\right)\frac{1}{(h_s+\tau v)}\rho\end{bmatrix} = \begin{bmatrix}0 \\ \frac{\rho\left(v_m\left(1-\frac{\rho}{\rho_m}\right)\right)-v}{\tau}\end{bmatrix}. \tag{31}$$

The vector form of the traffic models in Equation (26) in quasi-linear form is

$$\frac{\partial u}{\partial t} + \frac{A(u)\partial u}{\partial x} = 0 \tag{32}$$

where $A(u)$ is the Jacobian matrix, which denotes $\frac{\partial f}{\partial u}$ and helps approximate eigenvectors and eigenvalues. The eigenvalues then approximate the second-order partial differential traffic systems, which analyze the traffic behavior evolution.

From Equation (31), $A(u)$ for the proposed model is

$$\begin{bmatrix} 0 & 1 \\ -v^2 + \left(\frac{-0.03599+0.000314\rho}{-0.5979+0.0134v(\rho)}\right)\frac{1}{(h_s+\tau v)} & 2v \end{bmatrix} \tag{33}$$

To find the eigenvalues and eigenvectors from Equation (31), we use

$$|A(u) - \lambda I| = 0, \tag{34}$$

where I is the 2×2 identity matrix, and λ represents eigenvalues. From Equation (34), Equation (35) gives the quadratic relation of eigenvalues as

$$\lambda^2 - 2v\lambda + v^2 - \left[\left(\frac{-0.03599 + 0.000314\rho}{-0.5979 + 0.0134v}\right)\frac{1}{(h_s + \tau v)}\right]^2 = 0. \tag{35}$$

From Equation (35), the eigenvalues are given in Equation (36)

$$\lambda_{1,2} = v \pm \left(\frac{-0.03599 + 0.000314\rho}{-0.5979 + 0.0134v(\rho)}\right)\frac{1}{(h_s + \tau v)}, \tag{36}$$

which gives the velocity changes. That is, a change in traffic behavior is based on traffic emissions. To optimize the emissions, the coefficients of density and velocity can be controlled. To find the eigenvectors, we use

$$|A(u) - \lambda I|x = 0, \tag{37}$$

and $x = \begin{pmatrix} 1 \\ x_2 \end{pmatrix}$, which gives eigenvector e_1 as

$$e_1 = \begin{bmatrix} 1 \\ \nu + \frac{1}{h_s + \tau v}\left(\frac{-0.03599 + 0.000314\rho}{-0.5979 + 0.0134\nu(\rho)}\right) \end{bmatrix}.$$

Then, e_2 is

$$e_2 = \begin{bmatrix} 1 \\ \nu - \frac{1}{h_s + \tau v}\left(\frac{-0.03599 + 0.000314\rho}{-0.5979 + 0.0134\nu(\rho)}\right) \end{bmatrix}.$$

To obtain the average velocity, Δf is

$$\Delta \mathrm{f} = \begin{bmatrix} \Delta \mathrm{f}_1 \\ \Delta \mathrm{f}_2 \end{bmatrix} = A(u)\Delta u \tag{38}$$

$$\Delta \mathrm{f} = \begin{bmatrix} 0 & 1 \\ \left[\frac{1}{h_s + \tau v}\left(\frac{-0.03599 + 0.000314\rho}{-0.5979 + 0.0134\nu}\right)\right]^2 - \nu^2 & 2\nu \end{bmatrix} \begin{bmatrix} \Delta\rho \\ \Delta\rho\nu \end{bmatrix} = 0 \tag{39}$$

From Equation (39),

$$\Delta \mathrm{f}_2 = \left(-\nu^2 + \left[\frac{1}{h_s + \tau v}\left(\frac{-0.03599 + 0.000314\rho}{-0.5979 + 0.0134\nu(\rho)}\right)\right]^2\right)\Delta\rho + 2\nu\Delta\rho\nu. \tag{40}$$

where from Equation (31),

$$\mathrm{f}(u) = \begin{bmatrix} \mathrm{f}_1 \\ \mathrm{f}_2 \end{bmatrix} = \begin{bmatrix} \rho\nu \\ \frac{(\rho\nu)^2}{\rho} + \left[\frac{1}{h_s + \tau v}\left(\frac{-0.03599 + 0.000314\rho}{-0.5979 + 0.0134\nu(\rho)}\right)\right]^2\rho \end{bmatrix}, \tag{41}$$

and f $(u) = \begin{bmatrix} \Delta \mathrm{f}_1 \\ \Delta \mathrm{f}_2 \end{bmatrix}$ from Equation (41) is

$$\Delta \mathrm{f}\ (u) = \begin{bmatrix} \Delta \mathrm{f}_1 \\ \Delta \mathrm{f}_2 \end{bmatrix} = \begin{bmatrix} \Delta\rho\nu \\ \Delta\left(\frac{(\rho\nu)^2}{\rho} + \left[\frac{1}{h_s + \tau v}\left(\frac{-0.03599 + 0.000314\rho}{-0.5979 + 0.0134\nu(\rho)}\right)\right]^2\rho\right) \end{bmatrix}. \tag{42}$$

Then, we obtain

$$\Delta \mathrm{f}_2 = \Delta\left(\frac{(\rho\nu)^2}{\rho} + \left[\frac{1}{h_s + \tau v}\left(\frac{-0.03599 + 0.000314\rho}{-0.5979 + 0.0134\nu(\rho)}\right)\right]^2\rho\right). \tag{43}$$

Comparing Equation (40) with (43), the quadratic relation of velocity is

$$\nu^2\Delta\rho - 2\nu\Delta(\rho\nu) + \Delta\left(\rho\nu^2\right) = 0 \tag{44}$$

Thus, the solution of Equation (44) is

$$\nu = \frac{2\Delta(\rho\nu) + 2\sqrt{\left(\Delta\rho\nu\right)^2 - (\Delta\rho)\left(\Delta\rho\nu^2\right)}}{2\Delta\rho}. \tag{45}$$

$\Delta\rho v = \rho_{i+1}v_{i+1} - \rho_i v_i$, where the subscript i denotes the road segments. Furthermore, $\Delta\rho v^2 = \rho_{i+1}{v_{i+1}}^2 - \rho_i {v_i}^2$, and $\Delta\rho = \rho_{i+1} - \rho_i$; thus, Equation (45) takes the form

$$v_{i+\frac{1}{2}} = \frac{v_{i+1} + \sqrt{\rho_{i+1}} + v_i\sqrt{\rho_i}}{\sqrt{\rho_{i+1}} + \sqrt{\rho_i}}. \tag{46}$$

Equation (46) denotes the average velocity of the proposed model at i and $i+1$. The average density of the proposed model is the geometric mean of the density [27].

$$\rho_{i+\frac{1}{2}} = \sqrt{\rho_{i+1}\rho_i} \tag{47}$$

Zhang's model has the same average density and velocity as the proposed model. The computing array for the performance analysis of the traffic model was created by segmenting the solution domain spatially and temporally. The time step was equal to Δt, and a road segment had a width of Δx, which was the distance between adjacent points. Using $v_{i+\frac{1}{2}}$ and $\rho_{i+\frac{1}{2}}$, the temporal and spatial traffic behavior could be estimated over the entire road segment with the ROE decomposition scheme [29].

6. Simulation Results

The performance of the proposed and Zhang's models is presented in this section for periods of 75 s. In these simulations, the temporal and spatial traffic evolution on a 300 m circular road was considered to assess the worst traffic scenario [16]. The circular road was chosen as the traffic dynamics within the circle are easy to observe. In addition, the worst traffic scenario can be observed on a circular rather than a straight road. The time period was 0.5 s, while the distance length was 10 m to guarantee Courant–Friedrichs–Levy conditions [28]. The relaxation time was 1 s [16]. The safe distance headway was 15 m. The traffic for both the proposed and Zhang's models achieved Greenshield's equilibrium velocity (speed, Equation (11)) distribution during alignment [25]. The traffic density on the road was normalized between zero and one. The maximum velocity and density were 9 m/s and 1, respectively. The initial density condition was

$$\rho_0 = \begin{cases} 0.1 \; for \; x < 100 \\ 0.6 \; for \; 100 \leq \mathrm{x} \leq 200. \\ 0.1 \; for \; x > 200 \end{cases} \tag{48}$$

A drastic change in the initial density was considered to assess the traffic behavior of Zhang's and the proposed models. The simulation parameters for both models are summarized in Table 5.

Table 5. Simulation parameters for the proposed and Zhang's models.

Input Parameters	Values
Road length, x	300 m
Type of road	Circular Road
Total time of simulation	50 s
Time step, Δt	0.5 s
Distance step, Δx	10 m
Relaxation time, τ	1 s
Safe distance headway, h_s	15 m
Equilibrium velocity distribution, $v(\rho)$	Greenshield's
Maximum velocity, v_m	9m/s
Maximum density (normalized), ρ_m	1

The proposed model's density behavior on a 300 m road at 5 s, 15 s, 37.5 s, and 50 s is shown in Figure 12 and indicates that the density was smoothed over time. The density range at 5 s was from 0.07 to 0.62. At 0 m, it was 0.0948, and at 40 m, the density reduced to 0.075. Then, it increased to 0.097 at 70 m. At 110 m, the density marginally increased to 0.117, and again to 0.619 at 140 m, then marginally reduced to 0.583 at 190 m. At 240 m, it reduced to 0.107 and remained at 0.099 till 300 m. At 15 s, the range of traffic density was 0.1 to 0.64. At 0 m, it was 0.120, and at 140 m, it was reduced to 0.100. It increased to 0.64 at 160 m, and at 190 m, it marginally reduced to 0.57. The traffic density smoothly aligned to 0.140 at 300 m. At 37.5 s, the range of traffic density was from 0.120 to 0.420. At 0 m, it was 0.300, which smoothly aligned to 0.120 at 200 m. The density increased to 0.410 at 225 m and marginally increased again to 0.420 at 235 m. The density decreased to 0.310 at 300 m. At 50 s, the range of traffic density was from 0.13 to 0.36. At 0 m, it was 0.35 and smoothly aligned to 0.13 at 250 m. The density decreased to 0.37 at 275 m and was uniform up to 300 m. The density of the proposed model was in the employed limits of zero and one.

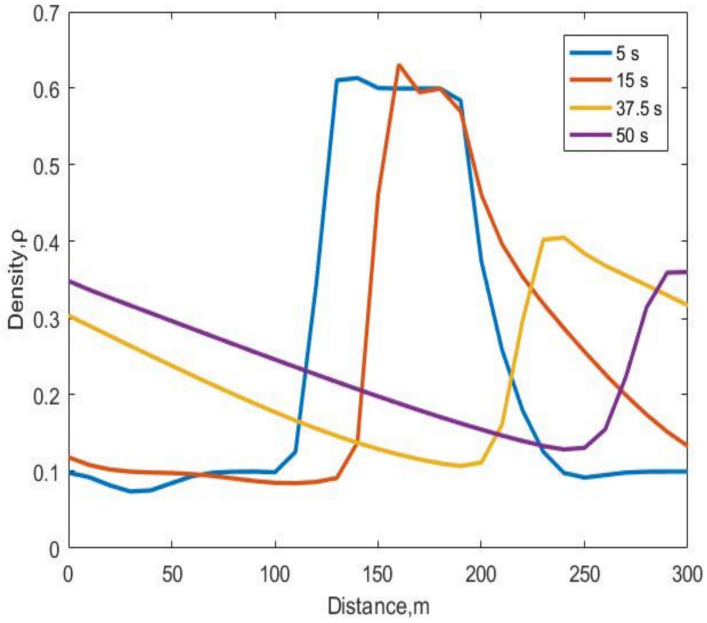


Figure 12. The behavior of the proposed model density on a 300 m circular road at 5 s, 15 s, 37.5 s, and 50 s.

The corresponding velocity behavior of the proposed model on a circular 300 m road at 5 s, 15 s, 37.5 s, and 50 s are shown in Figure 13. At 5 s, the velocity range was from 8.3 m/s to 3.6 m/s. At 0 m, it was 8.14 m/s. It was reduced from 8.32 m/s at 40 m to 8.13 m/s at 70 m. At 110 m, the velocity marginally decreased to 7.94 m/s and was further reduced to 3.49 m/s at 140 m. The velocity marginally increased to 3.72 m/s at 190 m and rose further to 7.98 m/s at 240 m. It remained uniform at 8.10 m/s up to 300 m. At 15 s, the velocity range was from 3.47 m/s to 8.28 m/s. At 0 m, it was 7.90 m/s, then marginally increased to 8.28 m/s at 140 m. It was reduced to 3.47 m/s at 160 m. At 190 m, the velocity increased to 3.8 m/s, then smoothly increased to 7.8 m/s at 300 m. At 37.5 s, the traffic velocity range was from 5.30 m/s to 8.00 m/s. At 0 m, it was 6.30 m/s and marginally increased to 8.00 m/s at 190 m. It decreased to 5.30 m/s at 240 m and then increased smoothly to 6.10 m/s at 300 m. At 50 s, the range of traffic velocity was from 5.7 m/s to 7.80 m/s. At 0 m, the velocity was 5.80 m/s, marginally increased to 7.80 m/s at 240 m, decreased to 5.80 m/s at 290 m, and was finally reduced to 5.70 m/s at 300 m. The proposed model velocity was in the range of 0 to 9 m/s.

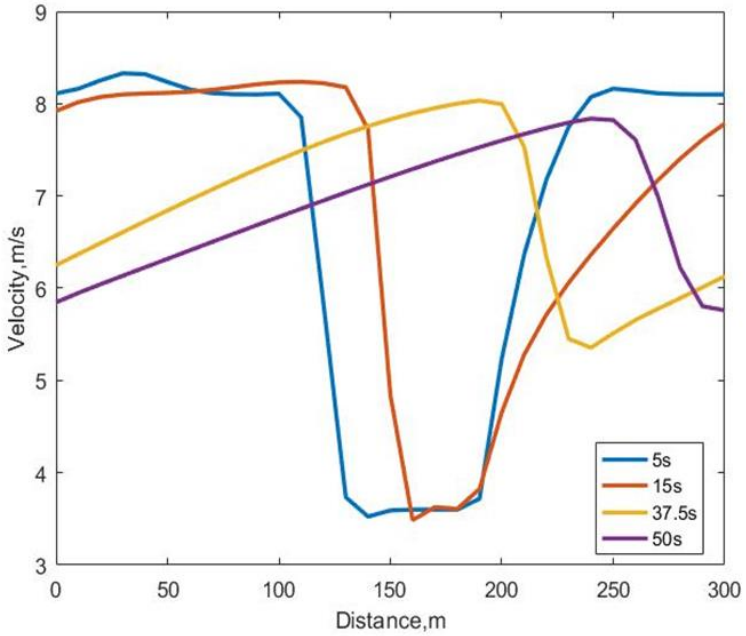


Figure 13. Velocity behavior of the proposed model on a 300 m circular road at 5 s, 15 s, 37.5 s, and 50 s.

The traffic behavior of Zhang's density model on a circular 300 m road at 5 s, 15 s, 37.5 s, and 50 s is shown in Figure 14. At 5 s, the range of traffic density was from 0.05 to 0.45. The density increased from 0.093 at 0 m to 0.43 at 170 m, then smoothly decreased to 0.154 from 170 m up to 260 m. The density was more oscillatory and abruptly changed over short distances between 240 m and 300 m, as shown in Figure 13. At 15 s, the range of density was from 0.16 to 0.32. The density reduced from 0.21 at 0 m to 0.16 at 60 m. It oscillated over a short distance of 10 m and increased between 60 m and 160 m. It rose to 0.32 at 200 m and fell to 0.24 at 300 m. At 37.5 s, the range of density was from 0.24 at 0 m to 0.23 at 140 m. At 50 s, the range of density was from 0.24 at 0 m to 0.25 at 70 m. The oscillatory behavior was observed with Zhang's model at 5 s and 15 s, as shown in Figure 14.

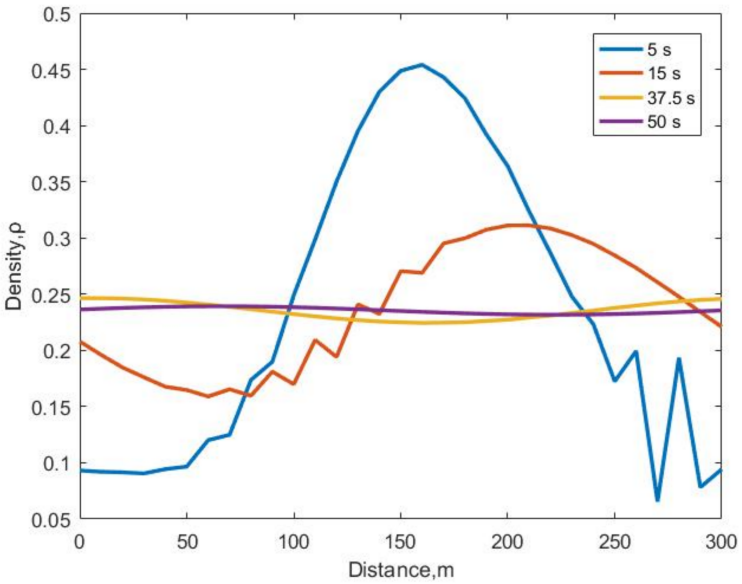


Figure 14. The Zhang model's density behavior on a 300 m circular road at 1 s at 5 s,15 s, 37.5 s, and 50 s.

The corresponding velocity of Zhang's model on a circular 300 m road at 5 s, 15 s, 37.5 s, and 50 s is shown in Figure 15. At 5 s, the velocity range was from 12.6 m/s to −1.5 m/s,

oscillating from 8.32 m/s at 0 m to 3.89 m/s at 100 m. The velocity decreased from 4.05 m/s at 110 m to 10.61 m/s at 270 m. At 280 m, the velocity was negative, −1.50 m/s, and at 290 m, it was 12.60 m/s. At 15 s, the velocity ranged between 8.10 m/s at 0 m and 5.5 m/s at 120 m. It oscillated over a short distance of 10 m from 60 m to 160 m and smoothly aligned from 6.0 m/s at 160 m to 7.8 m/s at 300 m. At 37.5 s and 50 s, the velocity was nearly at 6.8 m/s. The velocity behavior of Zhang's model was unusual as a velocity cannot be negative, and it did not stay within the prescribed range. Furthermore, changes over a shorter distance of 10 m did not accurately reflect traffic behavior.

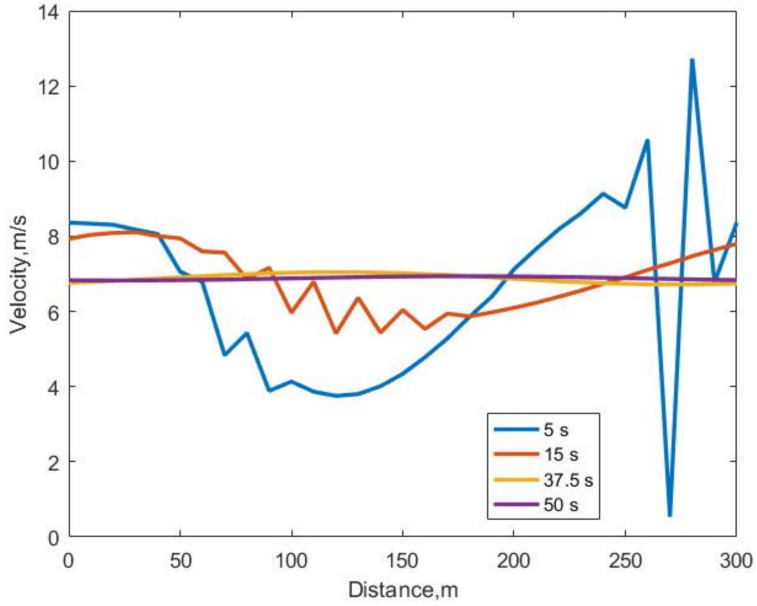


Figure 15. The Zhang model's velocity behavior on a 300 m circular road at 1 s at 5 s,15 s, 37.5 s, and 50 s.

Figure 16 shows the proposed model density behavior on a 300 m circular road for 75 s. The density varied from 0.07 to 0.62 within the minimum of zero and maximum of one range. Figure 17 shows the Zhang model's density compared with the proposed model's density behavior during 75 s. The Zhang model's density behavior was more oscillatory prior to the 50th time step than in the proposed model.

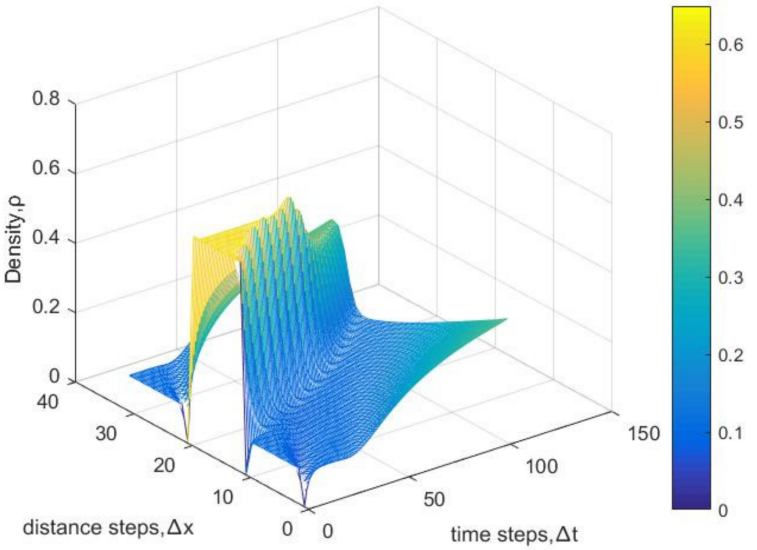


Figure 16. Density behavior of the proposed model over a 300 m circular road at different time steps during 75 s.

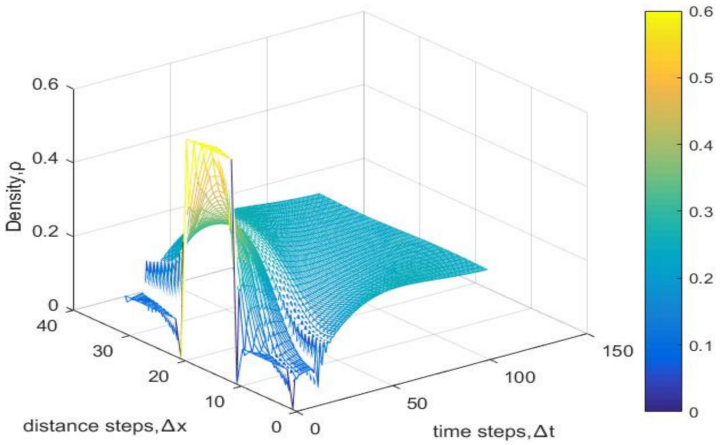


Figure 17. The Zhang model's density behavior over a 300 m circular road at different time steps during 75 s.

Figure 18 shows the proposed model velocity behavior over a 300 m circular road for 75 s. The velocity ranged from 3.6 m/s to 8.3 m/s. The variation in velocity shown in Figure 17 corresponds to the density behavior in Figure 16. The velocity was within the prescribed minimum of 0 m/s and a maximum of 9 m/s. Figure 19 compares the velocity behavior of the proposed and Zhang's models. The velocity ranged from −1.5 m/s to 12.6 m/s, which was an oscillatory and unusual behavior. The traffic velocity over the distance cannot be negative with time. The velocity of Zhang's model prior to the 50th time step did not stay within the employed range. For example, at the 50th distance step and 10th time step, Zhang's model gave a velocity of 8.1 m/s, while the proposed model gave a velocity of 8.3 m/s. This suggests that both models provided comparable velocity predictions, with the proposed model slightly exceeding the Zhang model's value. At the 200th distance step and 10th time step, Zhang's model gave a velocity of 6.4 m/s, as shown in Figure 17, while the proposed model's velocity was 3.7 m/s, as shown in Figure 18. This indicates that both models provided similar velocity predictions but with the proposed model's velocity values being lower than those of Zhang's model. However, at the 250th distance step and 10th time step, Zhang's model gave a velocity of 9.1 m/s, exceeding the maximum expected velocity value of 9 m/s, as shown in Figure 17. Thus, in some cases, Zhang's model provided higher velocity predictions than the expected maximum. The density and velocity for Zhang's and the proposed models at the 10th time step (5 s) for a 300 m road are summarized in Table 6.

Table 6. Comparison of Zhang's and the proposed models' density and velocity behavior for the 300 m road at the 10th time step.

S. No	Distance Step (Δx) and Time Step (Δt = 10)	Zhang's Model		Proposed Model	
		Density	Velocity (m/s)	Density	Velocity (m/s)
1	Δx = 50	0.094	8.10	0.075	8.30
2	Δx = 100	0.190	0.19	0.099	8.10
3	Δx = 150	0.430	4.01	0.610	3.50
4	Δx = 200	0.390	6.40	0.500	3.70
5	Δx = 250	0.220	9.10	0.098	8.10
6	Δx = 300	0.078	6.70	0.099	8.10

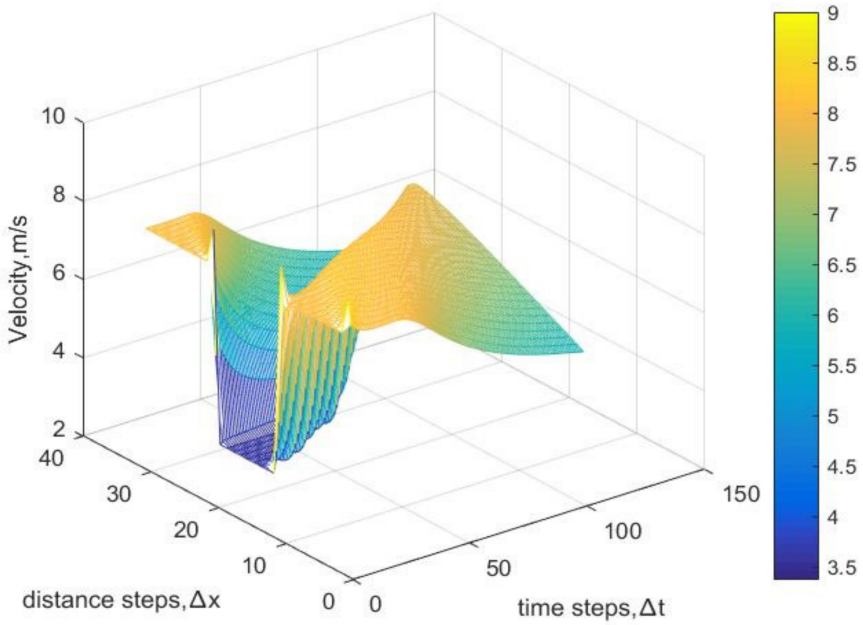


Figure 18. Velocity behavior of the proposed model over a 300 m road based on emissions.

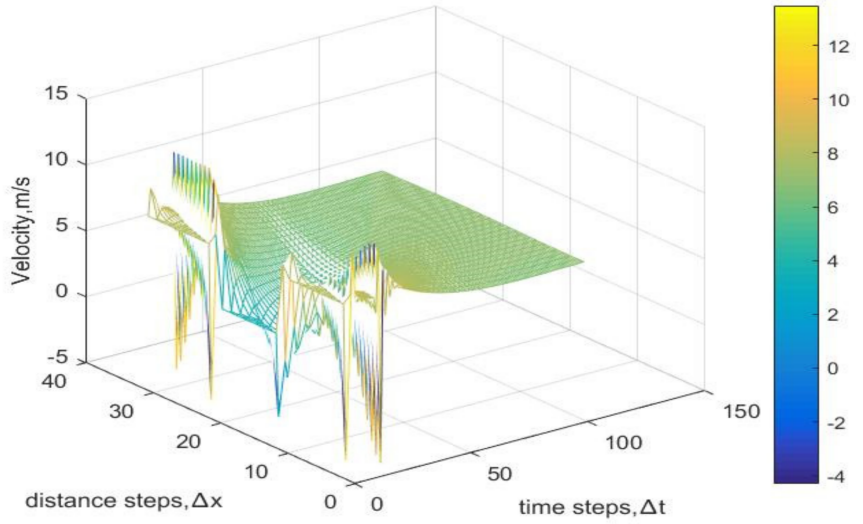


Figure 19. The Zhang model's velocity behavior over a 300 m road.

With Zhang's model, the changes in velocity were significant, while the proposed model showed minor changes in velocity, as shown in Table 7, suggesting that the Zhang model's velocity behavior was more oscillatory and unrealistic. Thus, Zhang's model inadequately characterized traffic behavior. Furthermore, the proposed model took into account traffic emissions and could, therefore, make traffic emission predictions, while Zhang's model could not. In the proposed model, as the velocity increased, the emissions decreased, as expected. For example, at the 100th distance step and 10th time step, the emission value, based on velocity in the proposed model, was 8.7 kg CO_2/km. Based on the correct depiction of the corresponding density behavior shown in Figure 17, the proposed model's lower velocity resulted in more accurately calculated lower emissions. Furthermore, the Zhang model's velocity behavior in Figure 19 did not correspond to the density behavior shown in Figure 17, as a high velocity beyond the maximum was predicted for a lower density. The emission values based on velocity for the proposed model at the 10th time step (5 s) for a 300 m road are summarized in Table 7.

Table 7. Comparison of the CO_2 emissions based on the velocity estimated by Zhang's model and the proposed model.

S. No	Distance Step (Δx) and Time Step (Δt = 10)	Proposed Model		
		Velocity (m/s)	Velocity (m/s)	Emissions (kg CO_2/km)
1	Δx = 50	8.10	8.32	8.60
2	Δx = 100	0.18	8.10	8.70
3	Δx = 150	4.01	3.50	11.10
4	Δx = 200	6.40	3.70	11.00
5	Δx = 250	9.10	8.00	8.70
6	Δx = 300	6.70	8.10	8.70

The results in Table 7 suggested that the proposed model could mitigate the velocity, traffic density, and vehicle emissions in dynamic traffic management.

7. Conclusions

In this paper, vehicle CO_2 emission models based on equilibrium velocity and density were developed through regressive techniques using data acquired with the help of engine onboard diagnostic units from vehicles moving on the road. The emissions regression models were integrated with Zhang's model, and a new macroscopic traffic model that included traffic emissions was proposed. The traffic speed and density predicted by the proposed model could provide the details of vehicle emissions. The spatial and temporal evolutions of the suggested model were compared with those of Zhang's model at various time steps. The analysis of the results considered the worst traffic scenario on a circular 300 m road. Simulation results showed that Zhang's model failed to remain within the predefined maximum 9 m/s and minimum 0 m/s velocity. The proposed model's velocity and density, which were based on traffic emissions, remained within the prescribed limits. In addition, the proposed model could predict emissions based on traffic velocity and could be optimized for pollution mitigation. The unrealistic traffic behavior of Zhang's model was due to inadequate traffic characterization. Zhang's model considered the traffic's spatial and temporal evolution based on the changes in velocity, while the proposed model obtained practical data from the roadside and could therefore more accurately characterize the precise traffic behavior. That is, the proposed model considered the changes in density based on directly obtained emissions data. The maximum emissions occurred at lower velocities and were lower at higher velocities, as predicted by the proposed model. Further, the integration of traffic emissions and driver presumptions in the proposed model was established on the basis of physical traffic parameters.

The proposed model could manage traffic control, congestion, and pollution, while Zhang's model was inadequate for these purposes.

Author Contributions: Conceptualization, T.Q., A.B.A., K.S.K. and Z.H.K.; methodology, T.Q., A.B.A., F.A.K. and K.S.K.; software, A.B.A., M.A. and A.A.; validation, T.Q., Z.H.K., K.S.K., F.A.K. and A.A.; formal analysis, T.Q., Z.H.K. and K.S.K.; investigation, T.Q., A.B.A., F.A.K. and W.K.; resources, Z.H.K., A.B.A., K.S.K. and F.A.K.; data curation, K.S.K., Z.H.K., A.B.A. and M.A.; writing—original draft preparation, T.Q. and A.B.A.; writing, T.Q., A.B.A., Z.H.K., K.S.K. and M.A., review and editing, Z.H.K., T.Q., A.B.A., M.A., A.A. and W.K.; visualization, T.Q., M.A., A.A. and A.B.A.; supervision, Z.H.K. and F.A.K.; project administration, F.A.K., K.S.K. and A.B.A.; funding acquisition, A.B.A., Z.H.K., M.A., A.A. and W.K. All authors have read and agreed to the published version of the manuscript.

Funding: This research has been funded by Scientific Research Deanship at University of Ha'il—Saudi Arabia through project number RG-22 020.

Institutional Review Board Statement: Not applicable.

Informed Consent Statement: Not applicable.

Data Availability Statement: The data is not publicly available.

Conflicts of Interest: The authors declare no conflict of interest.

References

1. Fuller, R.; Sandilya, K.; Hanrahan, D. Pollution and Health Metrics. 2019. Available online: https://gahp.net/pollution-and-health-metrics/ (accessed on 7 July 2022).
2. EPA. Sources of Greenhouse Gas Emissions. 2020. Available online: https://www.epa.gov/ghgemissions/sources-greenhouse-gas-emissions (accessed on 8 July 2022).
3. EEA. EEA Greenhouse Gas Data Viewer Information. 2021. Available online: https://www.eea.europa.eu/data-and-maps/data/data-viewers/greenhouse-gases-viewer (accessed on 8 July 2022).
4. Luo, Z.; Wan, G.; Wang, C.; Zhang, X. *Pollution and Road Infrastructure in Cities of the People's Republic of China*; ADBI Working Paper; Asian Development Bank Institute: Tokyo, Japan, 2017; Available online: https://www.adb.org/publications/pollution-and-road-infrastructure-cities-prc (accessed on 22 July 2022).
5. Ahn, K. Microscopic Fuel Consumption and Emission Modeling. Ph.D. Thesis, Virginia Tech, Blacksburg, VA, USA, 1998.
6. Abo-Qudais, S.; Qdais, H.A. Performance evaluation of vehicles emissions prediction models. *Clean Technol. Environ. Policy* **2005**, *7*, 279–284. [CrossRef]
7. Smit, R.; Ntziachristos, L.; Boulter, P. Validation of road vehicle and traffic emission models—A review and meta-analysis. *Atmos. Environ.* **2010**, *44*, 2943–2953. [CrossRef]
8. Evans, L.; Herman, R. Automobile Fuel Economy on Fixed Urban Driving Schedules. *Transp. Sci.* **1978**, *12*, 137–152. [CrossRef]
9. Akcelik, R.; Biggs, D.C. A discussion on the paper on fuel consumption modeling by Post et al. *Transp. Res. Part B* **1985**, *19*, 529–533. [CrossRef]
10. André, M. The ARTEMIS European driving cycles for measuring car pollutant emissions. *Sci. Total Environ.* **2004**, *334–335*, 73–84. [CrossRef] [PubMed]
11. Richards, P.I. Shock Waves on the Highway. *Oper. Res.* **1956**, *4*, 42–51. [CrossRef]
12. Helbing, D. Gas-kinetic derivation. *Phys. Rev. E Vol.* **1996**, *53*, 2366–2381. [CrossRef] [PubMed]
13. Caligaris, C.; Sacone, S.; Siri, S. On the Payne-Whitham differential model stability constraints in one-class and two-class cases. *Appl. Math. Sci.* **2010**, *4*, 3795–3821.
14. Mohan, R.; Ramadurai, G. Heterogeneous traffic flow modelling using second-order macroscopic continuum model. *Phys. Lett. Sect. A Gen. At. Solid State Phys.* **2017**, *381*, 115–123. [CrossRef]
15. Khan, Z. Traffic Modelling for Intelligent Transportation Systems. Ph.D. Thesis, University of Victoria, Victoria, BC, Canada, 2016.
16. Khan, Z.H.; Gulliver, T.A. A macroscopic traffic model based on transition velocities. *J. Comput. Sci.* **2020**, *43*, 101131. [CrossRef]
17. Zhang, H.M. A theory of nonequilibrium traffic flow. *Transp. Res. Part B Methodol.* **1998**, *32*, 485–498. [CrossRef]
18. Aw, A.; Rascle, M. Resurrection of "second order" models of traffic flow. *SIAM J. Appl. Math.* **2000**, *60*, 916–938. [CrossRef]
19. Daganzo, C.F. Requiem for second-order fluid approximations of traffic flow. *Transp. Res. Part B* **1995**, *29*, 277–286. [CrossRef]
20. Sohail, A.M.; Khattak, K.S.; Iqbal, A.; Khan, Z.H.; Ahmad, A. Cloud-based detection of road bottlenecks using obd-ii telematics. In Proceedings of the 2019 22nd International Multitopic Conference (INMIC), Islamabad, Pakistan, 29–30 November 2019. [CrossRef]
21. Zeb, A.; Khattak, K.S.; Agha, A.; Khan, Z.H.; Sethi, M.A.J.; Khan, A.N. on-Board Diagnostic (Obd-Ii) Based Cyber Physical System for Road Bottlenecks Detection. *J. Eng. Sci. Technol.* **2022**, *17*, 906–922.
22. Available online: https://docs.aws.amazon.com/ (accessed on 14 February 2023).
23. Meseguer, J.E.; Toh, C.K.; Calafate, C.T.; Cano, J.C.; Manzoni, P. Drivingstyles: A mobile platform for driving styles and fuel consumption characterization. *J. Commun. Netw.* **2017**, *19*, 162–168. [CrossRef]
24. Greenshields, B.D. A Study in Highway Capacity, Highway Research Board. *Proceedings* **1935**, *14*, 458.
25. Jin, W.L.; Zhang, H.M. Solving the Payne-Whitham traffic flow model as a hyperbolic system of conservation laws with relaxation. *Transp. Sci.* **2001**, *1*, 24.
26. Berg, P.; Mason, A.; Woods, A. Continuum approach to car-following models. *Phys. Rev. E-Stat. Phys. Plasmas Fluids Relat. Interdiscip. Top.* **2000**, *61*, 1056–1066. [CrossRef] [PubMed]
27. Roe, P.L. Approximate Riemann Solvers, Parameter Vectors, and Difference Schemes. *J. Comput. Phys.* **1981**, *43*, 357–372. [CrossRef]
28. Morgan, J.V. Numerical Methods for Macroscopic Traffic Models. Ph.D. Thesis, University of Reading, Reading, UK, August 2002.
29. Khan, Z.H.; Gulliver, T.A. A macroscopic traffic model for traffic flow harmonization. *Eur. Transp. Res. Rev.* **2018**, *10*, 30. [CrossRef]

Disclaimer/Publisher's Note: The statements, opinions and data contained in all publications are solely those of the individual author(s) and contributor(s) and not of MDPI and/or the editor(s). MDPI and/or the editor(s) disclaim responsibility for any injury to people or property resulting from any ideas, methods, instructions or products referred to in the content.